RSC Advances

PAPER

View Article Online
View Journal | View Issue

Cite this: *RSC Adv.*, 2024, **14**, 17664

Electro-chemical studies of Zn doped nickel oxide nanoparticles synthesized *via* solution combustion method using green and chemical fuels

N. Nasir Ahamed,[ab] Jayadev Pattar,*[b] M. R. Anil Kumar,[c] N. Basavaraju,[d] N. Raghavendra,[d] Sharanakumar T. M.,[e] C. R. Ravikumar [d] and H. C. Ananda Murthy *[fg]

Received 5th March 2024
Accepted 12th April 2024

DOI: 10.1039/d4ra01706d

rsc.li/rsc-advances

This study presents a new green solution combustion method (aloe vera gel extract as fuel) and chemical method (glucose as fuel) to synthesise Zn-doped nickel oxide nanoparticles (Zn:NiO NPs). The face centered cubic crystal structure (FCC) phase was validated by PXRD, while the produced samples' spongy, spherical, agglomerated, and porous characteristics were shown by electron microscopy. The energy band gap values of 4.21 eV and 4.09 eV, respectively, were deduced for green and chemically synthesized Zn:NiO NPs. The reversibility was demonstrated by cyclic voltammetry with a lower E_O–E_R value for the green-Zn:NiO electrode. The studies on electrochemical impedance confirmed strong conductivity for the NPs by demonstrating a low charge transfer resistance. The Zn:NiO NPs are easily convertible into a stable electrode material that may be used in supercapacitors. According to the findings, Zn:NiO is an economical and promising material for use in supercapacitors in the future.

Introduction

A p-type semiconductor with a small bandgap of 1.2 eV, nickel oxide (NiO) is a member of the group of transition metal oxides. With a high theoretical capacity (718 mA h g^{-1}), widespread availability, and a low cost, NiO stands out among the well-known metal oxides as a potential substitute for graphite[1] which is extensively investigated because of its promising applications of bulk and nanoparticles in recent years. Supercapacitors, solar panels, electrochemical glucose sensors, fuel cells, catalysts, gas detection devices, electrochromic smart windows, lithium ion batteries, and wastewater treatment for dye pollution were a few of the uses of NiO. NiO thin films have also been used in the dye-sensitized gas sensors, and opto-electronic devices.[2–16] The synthesized Mn, Fe, and Zn doped NiO nanoparticles boost several characteristics such as ferromagnetic nature, catalytic, and electrochemical efficiency, according to the particle size effect. It demonstrates that the doped NiO is extremely influenced by the factors such as, the synthesis technique, calcination temperature, and initial precursor as reported by Panigrahi *et al.*[19]

Zinc is prospective transition metal element that can be employed as a suitable strengthening component for nickel oxide as its ionic radius is close to that of Ni.[18] By adding more cations or by producing Ni^{2+} vacancies, the semiconducting characteristic can be achieved in the doped NiO.[19] In the oxide systems, which may be modified to add physical changes lattice vacancies are one of the most significant flaws reported by Madanakumara *et al.*[15] The nanoparticles of Zn-doped NiO are synthesized using a variety of physical and chemical techniques. The chemical co-precipitation, hydrothermal treatment, and solid-state thermal degradation are a few illustrations, permitting manipulation of particle size, dispersion, and form.[21,22] In this work, the solution combustion method was used to prepare the zinc oxide nanoparticles. The most efficient preparation technique in this study is combustion synthesis, which produces nano powders that are homogeneous in nature, very pure, and of excellent quality, and which can be stoichiometrically controlled. In addition, the effects of detection of analyte by NPs are the primary focus of the benefits, which include simplicity, high response rate, low cost and time savings, scalability, affordability, and narrow particle size dispersion.[23]

[a]*Department of Physics, Government College for Women, Chintamani-563125, India*
[b]*Department of Science, School of Applied Sciences, REVA University, Bangalore-64, India*
[c]*Department of Chemical and Materials Engineering, Gina Cody School of Engineering and Computer Science, Concordia University, Montreal, H3G 2W1, Canada*
[d]*Research Centre, Department of Chemistry, East West Institute of Technology, Bangalore-91, India. E-mail: ravicr128@gmail.com*
[e]*Department of Chemistry, Ballari Institute of Technology and Management, Bellary-583104, Karnataka, India*
[f]*Department of Applied Sciences, Papua New Guinea University of Technology, Lae, Morobe Province, 411, Papua New Guinea*
[g]*Department of Prosthodontics, Saveetha Dental College & Hospital, Saveetha Institute of Medical and Technical Science (SIMATS), Saveetha University, Chennai 600077, Tamil Nadu, India*

This study also investigates the electrochemical behaviour of an electrode constructed from the Zn-doped NiO NPs using a variety of fuel combinations. As a working electrode in electrochemical workstations, Teflon-coated electrodes are preferred over traditional coin cell electrodes due to their lower cost, ease of preparation, and superior results in cyclic voltammetry. We have made serious effort to search deeply into the Zn-doped NiO electrode characteristics which has improved our understanding of potential electrode materials for use in future energy storage systems.

Materials and methods

Extraction of aloe vera gel

One of the eco-friendly fuel options for the production of NiO nanoparticles is aloe vera gel (Fig. 1), the Barbados or Curaçao aloe (syn. aloe barbadensis Mill., Fam. Liliaceae) has been used in the traditional and social remedies for many years. To prepare the aloe vera extract, the gel-filled interior part of the leaves was squeezed out. In order to get the aloe vera gel from the plant, an outer layer of green had been sliced away. The inner portion of the gel was finely crushed and ground into a thin, uniform jelly used for the synthesis of NiO NPs.

Synthesis of Zn doped NiO nanoparticles by green method

Nanoparticles of zinc oxide doped with nickel (Zn:NiO NPs) were synthesized by burning an extract of aloe vera gel in a bio-mediated solution combustion chamber. 1 mL of aloe vera gel extract and stoichiometric volumes of $Ni(NO_3)_2 \cdot 6H_2O$ and $Zn(NO_3)_2 \cdot 6H_2O$ from Sigma Aldrich were combined in a beaker and vigorously mixed for 10 to 15 min using a magnetic stirrer. This mixture was placed in a pre-heated muffle furnace kept at 400 ± 10 °C. A clear gel was formed when the mixture was heated to the boiling point. Next, white foam was generated by the gel, and it grew until the container was full. A white powder with an exceptionally porous structure was left behind when the reaction was started somewhere inside the volume, with a flame appearing on the foam's surface and quickly spreading throughout. Nanoparticles of Zn:NiO were formed by a process that could self-propagate and withstand high temperatures. It took less than 5 min to finish the entire process. After further calcination at 500 °C for 3 h, the finished products were utilized for structural and other research.

Fig. 1 Aloe vera extract used for the preparation of nanopowders.

Synthesis of Zn doped NiO nanoparticles by chemical method

The rapid and straightforward self-ignited solution combustion synthesis (SCS) method was used to synthesize NiO NPs. A Petri dish was used to combine stoichiometric proportions of nickel(II) nitrate, zinc(II) nitrate, and glucose ($C_6H_{12}O_6$), a fuel, using a magnetic stirrer and a minimal amount of double-distilled water for 10 to 15 min. Then, the uniform mixture was put into a muffle furnace that had been warmed to around ~400 ± 10 °C. The process may generate Zn doped NiO NPs on its own and maintain high temperatures. It took less than 5 min to finish the entire process. After 3 h of further calcination at 500 °C, the finished products were utilized for structural and other investigations.

Nickel mesh electrode preparation for a galvanostatic charge–discharge study

The nickel working electrode was made by grinding a mixture of 75% Zn:NiO NPs powder, 15% graphite powder, and 10% polytetrafluoroethylene (PTFE) solution in an agate mortar for approximately 45 min, until a uniform thin sheet-type layer was achieved. The powder was created utilizing green and chemical fumes. The final product was then pasted on a nickel mesh. Applying a pressure of 20 MPa to the glued electrodes ensured a good electrical contact with the nickel mesh and active material. A final electrode with dimensions of 2 × 1 cm in area was achieved by insulating the backside of the electrode and a wire with a Teflon tape. To ensure proper contact with the electrolyte, it was immersed in a 0.1 N HCl solution for approximately 30 min prior to use.

Characterization

The PXRD analysis was carried out using a Shimadzu X-ray diffractometer (CuKα, 1.541 Å) at a scan rate of 2° per minute for the structural research. Using a Shimadzu (IR Affinity-1S) FTIR spectrometer in the 4000–400 cm^{-1} range, we can observe the presence of functional groups in the synthesized nanomaterials. Transmission electron microscopy (TEM) was used using a JEOL JEM-2100 (accelerating voltage up to 200 kV, LaB6 filament) to determine the three-dimensional morphology, polycrystallinity, and interplanar distance. Using the 200–800 nm range of the Shimadzu UV-vis spectrophotometer model 2600, the required diffuse reflectance spectral (DRS) tests. The CH Instruments (Electrochemical Analyzer Model 608E) was used to conduct the electrochemical impedance experiments using a tri-electrode setup.

Results and discussions

Dispersion of nanoparticles in a gel matrix has been one of the many crucial methods for addressing the aggregation problem. Aloe vera gel has good water solubility properties at moderate temperatures and is biodegradable. Besides, it is low-cost and has good stability at moderate synthesis temperatures. In this study, the aloe vera gel has been applied as a stabilizing matrix and reducing agent for the formation of Zn doped NiO NPs. The materials were synthesized by dissolving the host and dopant salt precursors at the same time following a solution combustion nanocrystal doping strategy.

PXRD analysis

The XRD patterns of Zn-doped NiO NPs prepared *via* chemical and green methods are shown in Fig. 2. The defects caused by the doping of Zn into the NiO crystal lattice vary in size with the doped particle. Zn-doped NiO NPs were found to have *d*-spacing for the associated diffraction planes of (111), (200), (220), (311), and (222), which correspond to NiO peaks. The remaining is for Zn peaks, which are similar to those identified in JCPDS card data (01-080-0075) with space group ($P6_3mc$).[24] Both the chemical and green production techniques have successfully integrated Zn into the NiO lattice, as seen by the peaks of NiO, which suggests that the structure of NiO is cubic. The enhanced crystallinity of the processed samples is confirmed by the presence of high-intensity peaks.

FTIR studies

FTIR transmission spectra were recorded at room temperature in the 400–4000 cm^{-1} range for both pure and zinc-doped nickel oxide nanoparticles. In order to get the samples ready for FTIR analysis, the synthesized powder was compressed into a pellet and mixed with potassium bromide (KBr). The FTIR spectra of chemically and biogenically synthesized Zn-doped NiO NPs were used to evaluate the presence of various functional groups, as shown in Fig. 3. The O–H stretching vibrations produced a wide absorption band at 3440 cm^{-1} in the chemical combustion peak. For Ni-doped ZnO samples, the vibrations at 2358 cm^{-1} are ascribed to $-CH_2$ vibrations, which are caused by symmetric and asymmetric C–H bonds, while the vibrations at 1633 cm^{-1} are ascribed to H–O–H bending vibration modes.[25] The resonances of the O–H stretching band at around 1100 cm^{-1} (ref. 5) Ni–O stretching vibration mode is attributed to the band at 427 cm^{-1}.[26] The use of FTIR results has shown the formation of pristine and Zn-doped NiO nanoclusters, but in the green synthesized NPs, the alkene group is present because of aloe vera usage as a fuel and there are extra bands at 1433 cm^{-1} that are medium C–H bending from the methyl group, cm^{-1} that are strong C=C bending from alkenes that are mono substituted, and 831 cm^{-1} that are medium C=C bending from alkenes that are tri substituted.

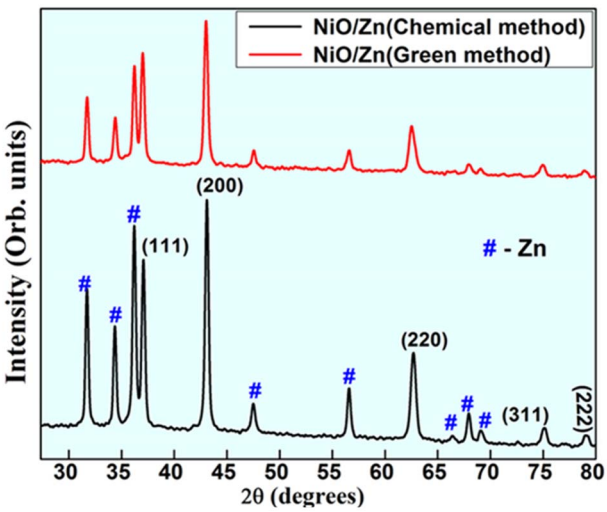

Fig. 2 PXRD patterns of Zn doped NiO NPs synthesized by solution combustion method.

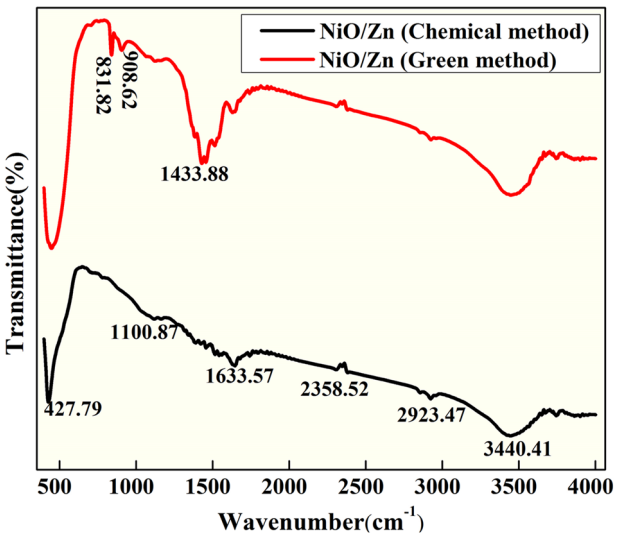

Fig. 3 FT-IR spectra of Zn-doped NiO NPs synthesized *via* green and chemical fuel.

The DRS analysis was used to study the conducting properties of synthesized Zn-doped NiO NPs produced using various fuels in the 200–800 nm range. In Fig. 4a, we can see the results of the DRS tests conducted on Zn-doped NiO NPs synthesized using the solution combustion method. Fig. 4b displays the band gap of these NPs. The relationships between the Zn-doped NiO NPs diffuse reflectance (R), absorption coefficient (K), and scattering coefficient (S) is measured using the Kubelka–Munk method are presented as eqn (1) and (2).[12,18]

$$F(R) = \frac{(1-R)^2}{2R} \quad (1)$$

$$F(R)h\nu = c_1(h\nu - E_g) \quad (2)$$

where, $F(R)$-Kubelka–Munk function and R-absolute reflectance of the sample and $h\nu$-light energy. The value of 'n' decides whether direct allowed transition ($n = 1/2$) or indirectly allowed transition ($n = 2$).[20,27] The Tauc relation for the energy band gap

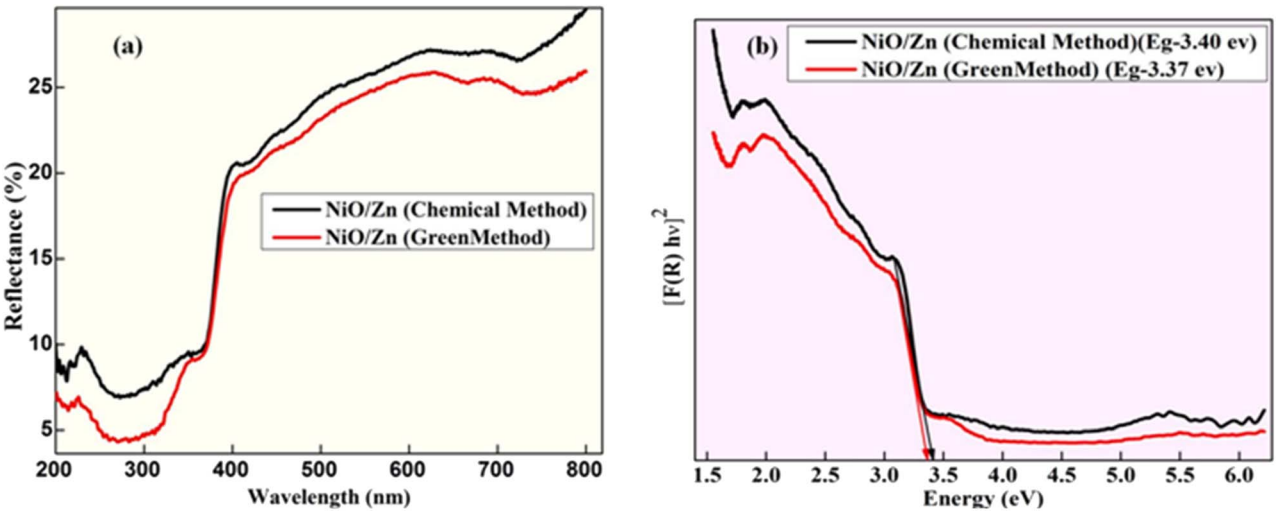

Fig. 4 (a) Diffuse reflection spectra of Zn-doped NiO NPs and (b) wood and Tauc plot to find energy band gap.

and the linear absorption coefficient (α) of a material, is given as eqn (3) and (4),

$$\alpha = \frac{(h\nu - E_g)^{\frac{1}{2}}}{h\nu} \quad (3)$$

$$[F(R)h\nu]^2 = c_2[h\nu - E_g] \quad (4)$$

The bandgap energy values of Zn-doped NiO NPs obtained from the chemical and green methods were found to be 3.40 eV and 3.37 eV, respectively, as shown in Fig. 4b, and the value of E_g was derived by extrapolating the linearly fitted areas from the $[F(R)h\nu]^2$ *versus* $h\nu$ plot. The oxygen vacancies are responsible for the distinctive features of photocatalytic applications, including a narrowing of the band gap.[28,29] Since the effective width of the forbidden band (E_g) directly impacts the charge transfer and improves electrochemical characteristics, it stands to reason that an increase in E_g should follow a drop in crystallite size.

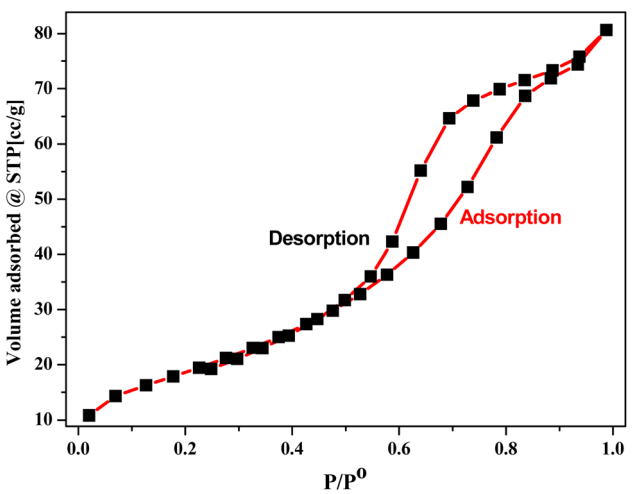

Fig. 5 The N_2 adsorption/desorption isotherms of green synthesized Zn doped NiO NPs.

BET studies

The ambient pressure gas sorption isotherm was measured using NOVA-1000 ver. 3.70 adsorption equipment. The surface area of a material is very crucial for catalytic applications. For the synthesized photocatalysts, the surface area calculated through the N_2 adsorption/desorption isotherm BET method was found to be 100.119 $m^2\ g^{-1}$ (Fig. 5). The mean pore diameter and mean pore volume were estimated to be 4.602 nm and 0.148 cc g^{-1} respectively. A higher specific surface area could provide more electrochemical reaction sites, which can increase the utilization of the electroactive materials.[1] The recorded type IV isotherm of green-Zn doped NiO hysteresis loops indicates a mesoporous structure for the material.

Microscopic studies

Fig. 6 displays TEM images of Zn-doped NiO NPs made using the combustion technique with chemical fuel. The TEM images, displayed in Fig. 6(a and b) at various 5 nm and 50 nm magnifications, reveal structures that are either hexagonal or orthorhombic.[4] The highly agglomerated particle structure is clearly visible in the TEM image, which is a hallmark of combustion-synthesized products. Fig. 6c shows the SAED pattern, which demonstrates that the NPs are polycrystalline and exhibit EDAX. The SAED pattern is characterized by a unique ring. According to energy dispersive spectroscopy, which is shown in Fig. 6d,[18] the sample is pure since it only contains Ni, Zn, and O. Fig. 7 displays a transmission electron micrograph of Zn-doped NiO nanoparticles made using the combustion technique using aloe vera gel as the fuel. Fig. 7(a and b) show that the green combustion approach preserves the same structure, including orthorhombic and hexagonal formations. Its polycrystalline nature is confirmed by SAED in Fig. 6c. The produced sample's purity and EDAX elemental

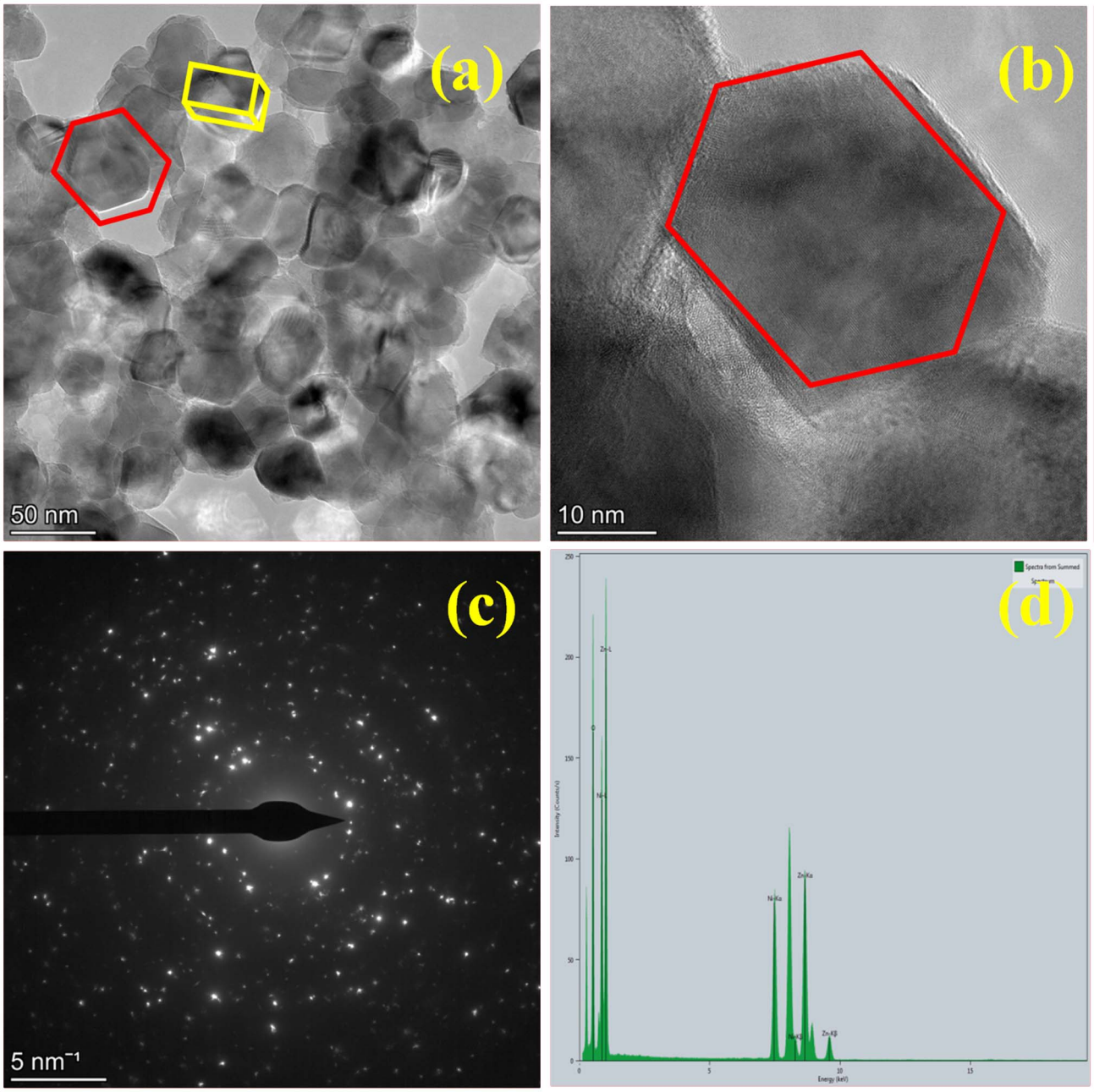

Fig. 6 Synthesized sample by chemical method in (a and b). TEM image of different magnification. (c). SAED. and (d). EDAX.

composition are displayed in Fig. 7d. Two different sources utilizing both materials for various purposes is shown by the similar features and elemental composition shown in the TEM, SEAD, and elemental analysis (EDAX) structures of the chemical approach and the green method.

SEM images of Zn-doped NiO NPs synthesized by chemical and green methods as depicted in Fig. 8. Fig. 8(a and c) reveal 1 micro meter magnification with voids, pores and non-uniform agglomerated morphology, for the NPs prepared by solution combustion method. SEM-EDX confirmed the synthesized Zn-doped NiO NPs containing several elements, including Ni, O, and Zn, as shown in Fig. 8(b and d).[30] Fig. 8 shows the elemental composition of both green and chemically synthesized Zn doped NiO NPs.[10,26]

The produced nanomaterials, graphite powder, and binder (PTFE) were combined in an agate mortar for approximately 45 minutes, with a percentage ratio of 70 : 15 : 15%, in order to create working electrode. This produced a homogenous graphite and nanomaterial paste. To improve electrical contact, an active material is attached to the nickel mesh. The glued electrodes were compressed for three minutes at 20 MPa in order to enhance the contact. After immersing the electrode in a 0.1 N HCl solution for 30 minutes, the electrode made the best possible contact with the electrolyte. Teflon tape was used to

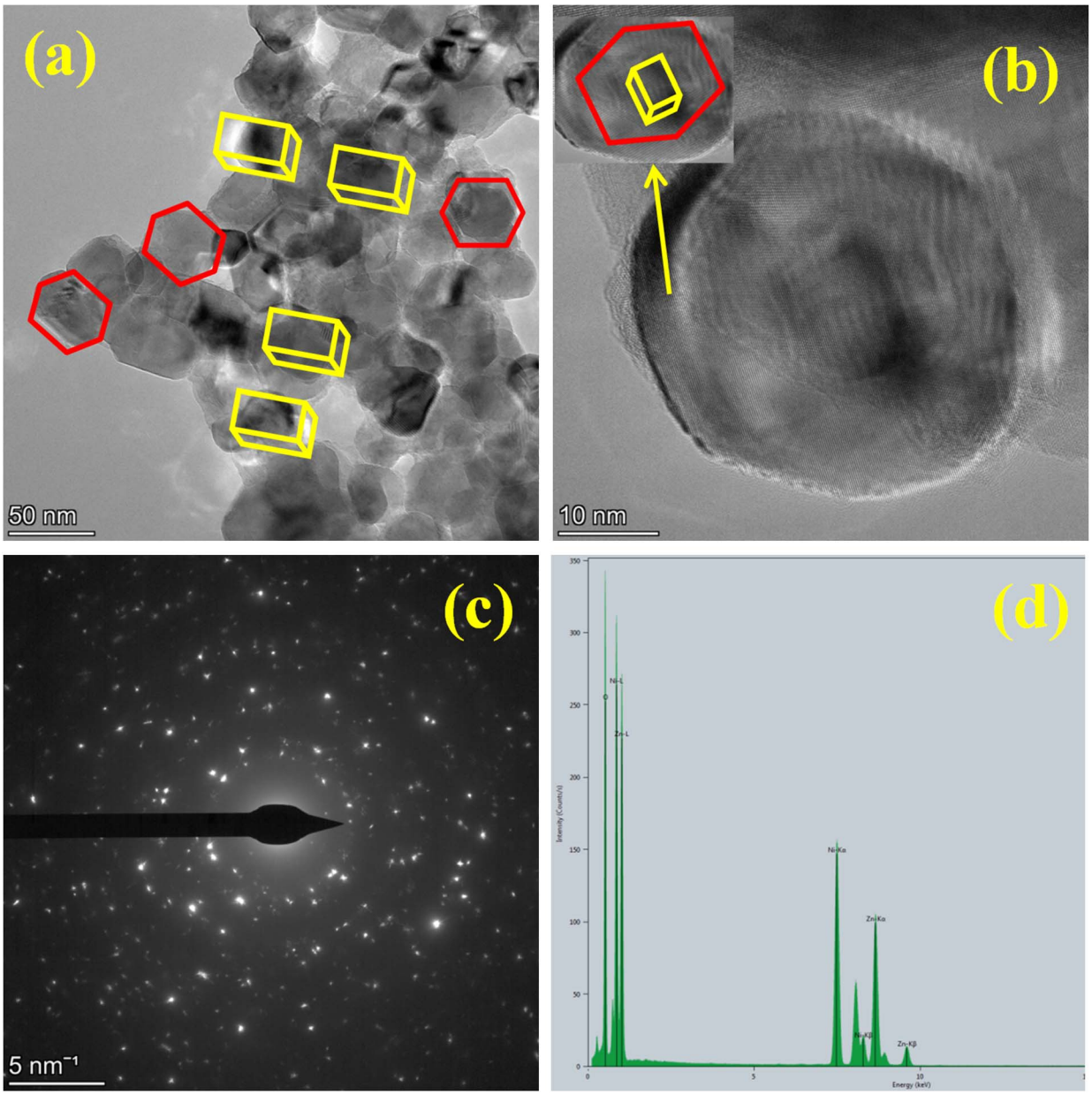

Fig. 7 Synthesized sample by green method in (a and b). TEM image of different magnification. (c). SAED. and (d). EDAX.

provide insulation for both the electrode and the other surface of the wire.

The cyclic voltammetry (CV) was utilized to assess the charge-holding capacity, charge–discharge cycles, reversibility reactions, and charging and discharging times in order to comprehend the excellent performance of the electrode (Fig. 9). The CVs were cycled between −0.3 V and 0.4 V (*vs.* Ag/AgCl). These studies yield valuable information about the redox behavior of the Zn Doped NiO electrode (chemical and green technique), which is crucial for the current inquiry. The redox process has a major role in the capacitance of the electrical double layer, as evidenced by the approximately rectangular form of the observed CVs.[15,31] The complete oxidation of nickel from +2 to +3 results in an electrode treated with additives that has a substantially higher capacity, allowing for effective use.[15]

Randles–Sevcik's formula (eqn (5)) for reversible processes[19] represents the height current as,

$$i_p = 2.69 \times 10^5 \times n^{3/2} \times A \times D^{1/2} \times C_0 \times v^{1/2} \quad (5)$$

where the number of electrons transferred in the reaction, the extent of the electrode, diffusion coefficient, scanning rate and initial concentration were denoted by n, A, D, ν, and C_0 respectively.

The correlation between the cathodic peak current (i_p) and the square root of the scan rate ($\nu^{1/2}$) is seen in Fig. 10. It appears that the reactions at the chemically and environmentally

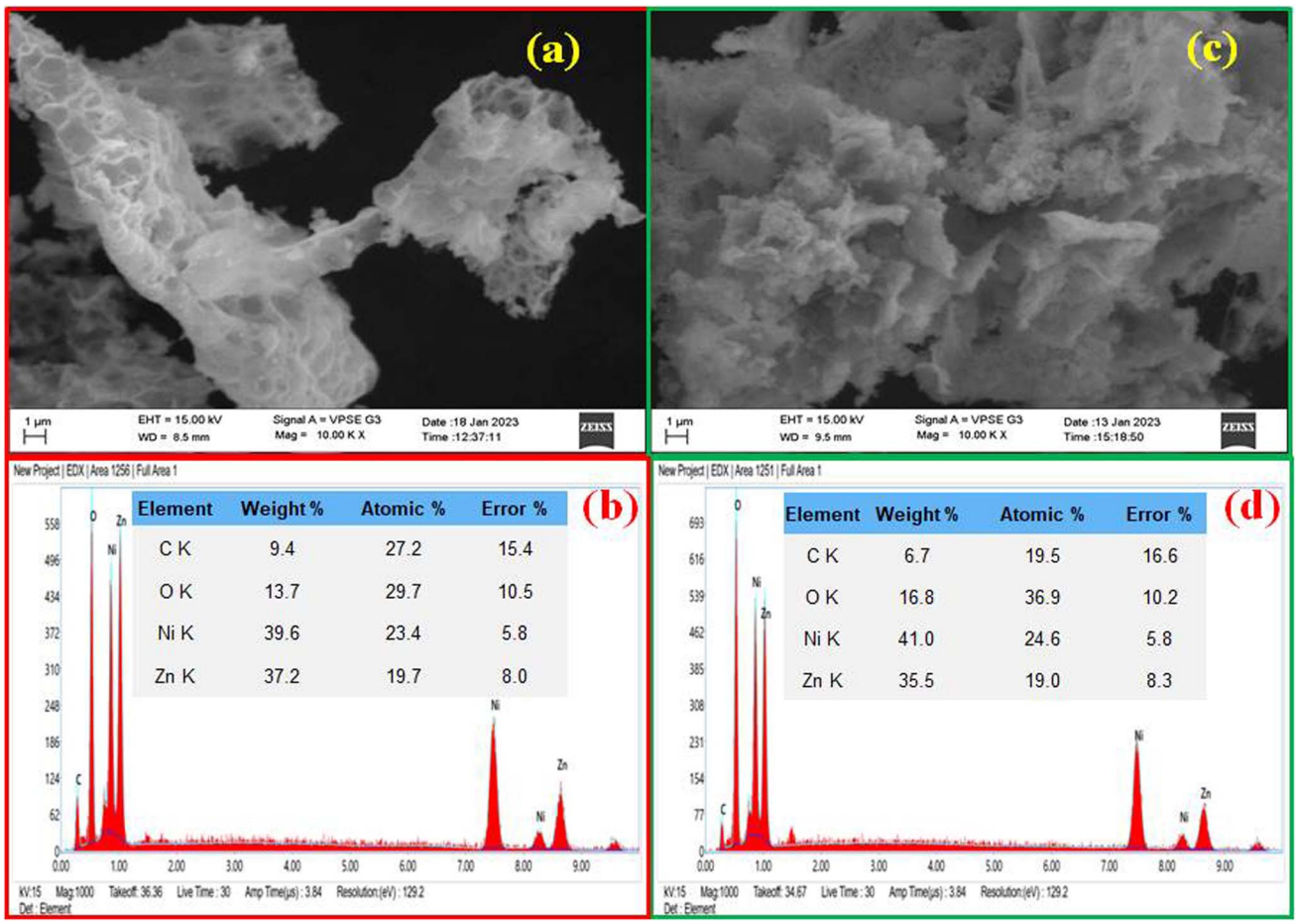

Fig. 8 (a) SEM images of Zn-doped NiO NPs synthesized *via* chemical fuel. (b) SEM-EDXNPs synthesized using chemical fuel (c) SEM images of Zn-doped NiO NPs synthesized using green fuel (d) SEM-EDX NPs synthesized using green fuel.

acceptable Zn-doped NiO electrodes are limited by hydrogen diffusion, as indicated by the straight-line link between ip and $\nu^{1/2}$. Our findings indicate that the proton diffusion coefficient is greater in the green Zn-doped NiO electrode material compared to the chemical Zn-doped NiO electrode. In comparison to the chemical Zn-doped NiO electrode material ($D = 7.245 \times 10^{-6}$ cm^2 s^{-1}), the proton diffusion coefficient for the green method of Zn-doped NiO electrode (5.589×10^{-5} cm^2 s^{-1})

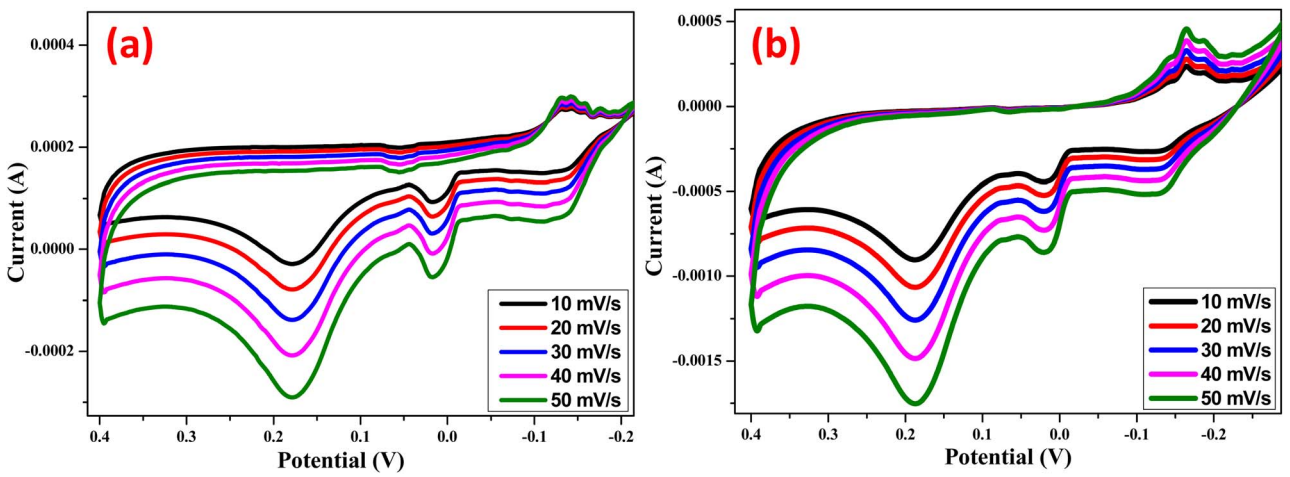

Fig. 9 Cyclic voltammogram of (a) Zn Doped NiO Chemical method (b) Zn doped NiO green method electrodes at different scan rates in 0.1 N HCl *vs* Ag/AgCl electrode.

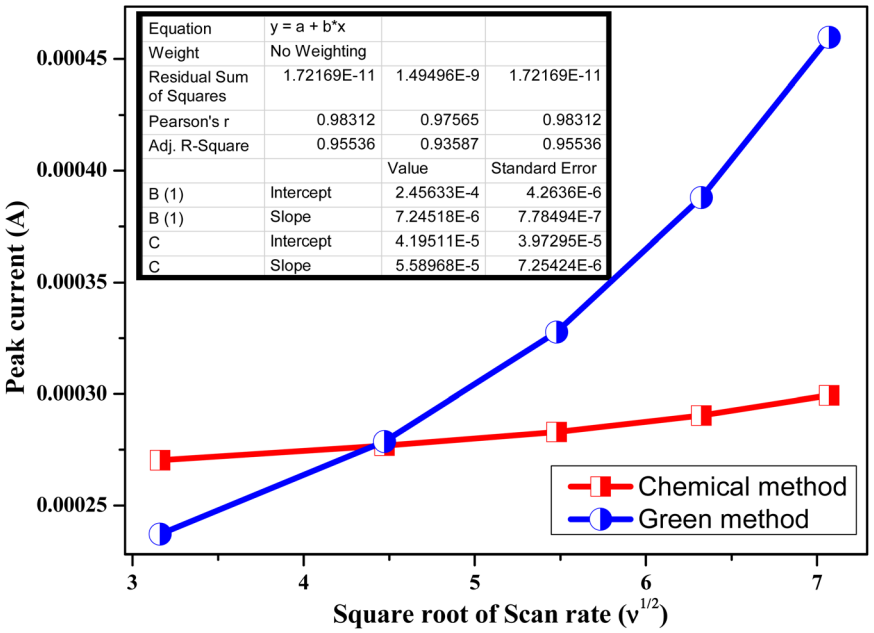

Fig. 10 Relationship between the anodic peak current (i_p) and the square root of the scan rate ($\upsilon^{1/2}$) for Zn Doped NiO electrodes prepared bychemical & green method.

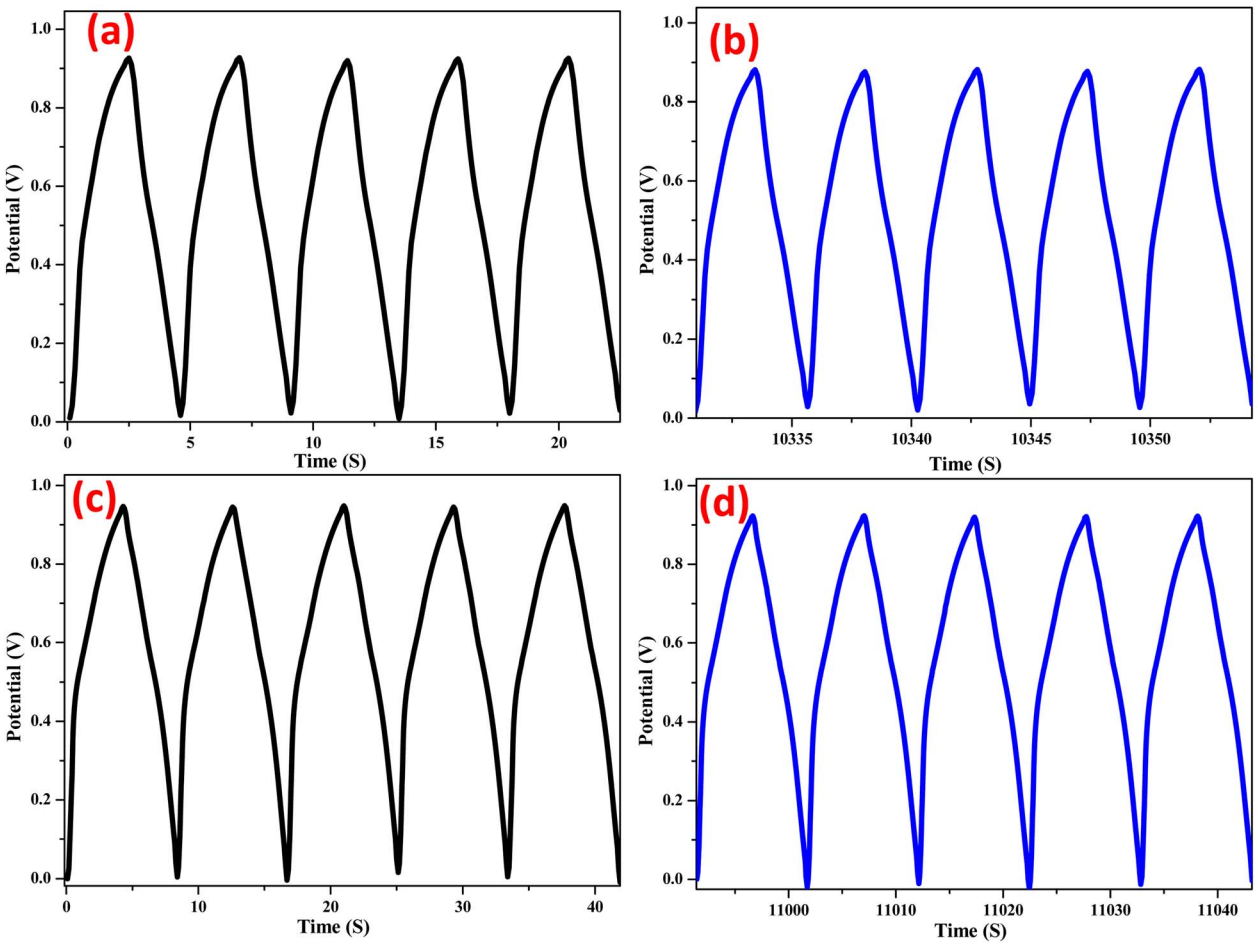

Fig. 11 Galvanostatic charge–discharge curve of Zn doped NiO in chemical method (a) first 5 cycles & (b) 2000th cycles and Zn doped NiO ingreen method (c) first 5 cycles & (d) 2000th cycles.

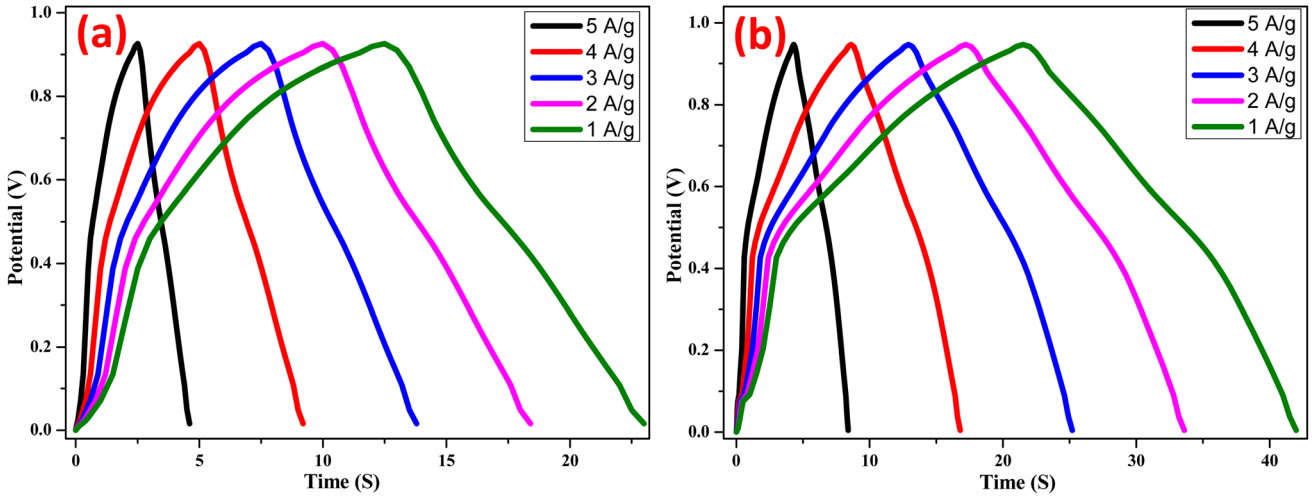

Fig. 12 Galvanostatic charge–discharge curves of (a) Zn doped NiO in chemical method (b) Zn doped NiO in green method at current densities varying from 1 to 5 A g^{-1}.

was found to be relatively higher by analyzing the slope of the fitted line in Fig. 10 and using eqn (5).

Fig. 11 and Fig. 12 shows the galvanostatic charge–discharge curves for NiO electrodes doped with Zn under both the chemical and green methods, at various current densities. Instead of a typical electric double-layer capacitor, the results show that the charge–discharge curves are more like a pseudo-capacitor. A larger amount of energy may be stored when the current density increases because the cumulative area along the current–potential axis grows. Using the formula (eqn (6)), we were able to determine the capacitance at each electrode.[17]

$$C = i \cdot \Delta t / m \Delta V \quad (6)$$

where, i, ΔV, Δt and m represent the applied currents, potential range, time of a discharge cycle, and mass of the Zn doped NiO electrodes in Chemical method and green method, respectively. From the equation the specific capacitance of the synthesized Zn doped NiO electrodes in chemical method and green method were found to be 368 and 385 F g^{-1}.

The electrochemical impedance spectra of Zn doped NiO electrodes (chemical and green) are shown in Fig. 13(a and b) before and after undergoing 2000 charge–discharge cycles. The electrode capacitance is shown as a straight line in low-frequency spectra, the Warburg resistance is shown as a slope in high-frequency spectra, and the electrode–electrolyte interface is shown to be depressed due to charge transfer resistance.[32,33] It is possible to determine the diameter of the semicircle arc on the real axis directly using charge-transfer resistance, it confirms that after charge–discharge enhancing the semicircle diameter and also movement of line towards X-axis shows lessening the capacitance and growing the resistance of the electrode. Finally, it can be concluded that the capacitance of green-Zn doped NiO electrode is higher than the chemical-Zn doped NiO electrode.

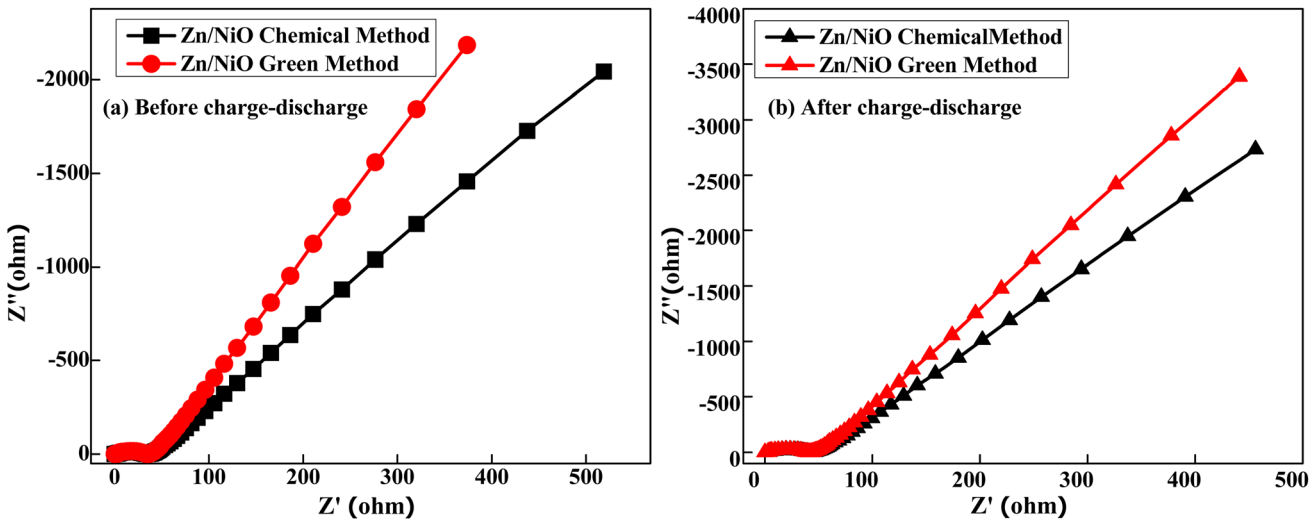

Fig. 13 Nyquist plot (a) before and (b) after charge–discharge of Zn doped NiO in Chemical and green method.

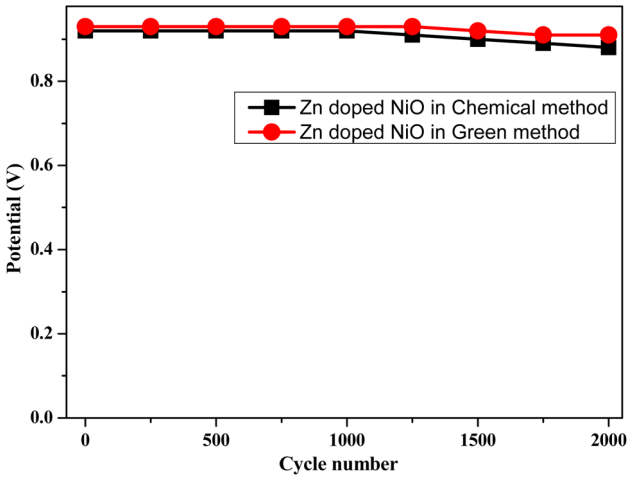

Fig. 14 Variation of potential with cycle numbers at a current density of 5 A g^{-1} of Zn doped NiO electrodes in chemical and green method.

The stability of a Zn doped NiO electrodes at a fixed current density (5 A g^{-1}) up to 2000 charge discharge cycles are shown in Fig. 14. After 1000 cycles, it can be seen that the voltage gradually drops for chemical-Zn doped NiO electrode. There is significant lessening in voltage up to 2000 cycles, with the electrode retaining 80% of its initial capacity. Similarly, green-Zn doped NiO electrode, there is no significant lessening in voltage up to 2000 cycles. This procedure suggested possibility that the electrode underwent a relaxation process, which would have improved performance and increased capacity retention.

Conclusions

The zinc doped NiO nanoparticles synthesised *via* chemical and green methods, exhibited remarkable morphological characteristics and enhanced electrochemical performance. These highly active and stable materials were utilized as electrodes in supercapacitors. The obtained specific capacitances of 368 F g^{-1} and 385 F g^{-1} for zinc doped NiO from the two approaches were attributed to the crystallinity, high specific surface area, and suitable pore size. These NPs exhibited Impressive cycling stability which was demonstrated as nearly 90% of the initial capacity was retained after 2000 cycles when sample prepared in green method. Additionally, this possesses the advantages of being cost-effective, environmentally friendly, and straight forward to manufacture.

Author contributions

The manuscript was written by contribution of all the authors and all authors approved the final version of the manuscript.

Conflicts of interest

There are no conflicts to declare.

References

1 J. K. Abhijeet and A. Dixit, *Sol. Energy*, 2022, **247**, 330–345.
2 J. Al Boukhari, L. Zeidan, A. Khalaf and R. Awad, *Chem. Phys.*, 2019, **516**, 116–124.
3 A. Khatri and P. S. Rana, *Phys. B*, 2020, **579**, 411905.
4 M. Ali, S. Sharif, S. Anjum, M. Imran, M. Ikram, M. Naz and S. Ali, *Mater. Res. Express*, 2019, **6**(12), 1250d5.
5 A. Samanta, M. N. Goswami and P. K. Mahapatra, *J. Alloys Compd.*, 2018, **730**, 399–407.
6 A. Kotta, E.-B. Kim, S. Ameen, H.-S. Shin and H. K. Seo, *J. Electrochem. Soc.*, 2020, **167**(16), 167517.
7 N. Basavaraju, S. C. Prashantha, H. Nagabhushana, C. Pratapkumar, C. R. Ravikumar, M. R. Anil Kumar, B. S. Surendra, T. R. ShashiShekhar, H. B. Premkumar and H. P. Nagaswarupa, *Ceram. Int.*, 2021, **47**(7), 10370–10380.
8 J. D. H. B. Chen, D. H. Bradhurst, S. X. Dou and H. K. Liu, *J. Electrochem. Soc.*, 1999, **146**(10), 3606.
9 G. ThiPhan, D. V. Pham, R. A. Patil, C.-H. Tsai, C.-C. Lai, W.-C. Yeh, Y. Liou and Y.-R. Ma, *Sol. Energy Mater. Sol. Cells*, 2021, **231**, 111306.
10 A. I. Inamdar, Y. S. Kim, J. S. Sohn, H. Im, H. Kim, D. Y. Kim and C. Park, *J. Korean Phys. Soc.*, 2011, **59**(1), 145–149.
11 A. Khorsand Zak, M. Ebrahimizadeh Abrishami, W. H. A. Majid, R. Yousefi and S. M. Hosseini, *Ceram. Int.*, 2011, **37**(1), 393–398.
12 C. R. Kumar, M. S. Santosh, H. P. Nagaswarupa, S. C. Prashantha, S. Yallappa and M. A. Kumar, *Mater. Res. Express*, 2017, **4**(6), 065503.
13 P. Kubelka and F. Munk, Einbeitragzuroptik der farbanstriche, *Z. Tech. Phys.*, 1931, **12**, 593–601.
14 Y. W. Li, J. H. Yao, C. J. Liu, W. M. Zhao, W. X. Deng and S. K. Zhong, *Int. J. Hydrogen Energy*, 2010, **35**(6), 2539–2545.
15 H. Madanakumara, H. S. Jayanna, C. V. Yelamaggad, S. Soundeswaran, M. Vishwas, K. S. Shamala, B. S. Surendra and N. Basavaraju, *Sensor. Int.*, 2022, **3**, 100193.
16 M. Palmer, M. Masikini, Li-W. Jiang, J.-J. Wang, F. Cummings, J. Chamier, O. Inyang and M. Chowdhury, *J. Alloys Compd.*, 2021, **853**, 156900.
17 R. T. Mouchou, T. C. Jen, O. T. Laseinde and K. O. Ukoba, *Mater. Today: Proc.*, 2021, **38**(2), 835–841.
18 M. Bagher Askari, P. Salarizadeh and A. D. Bartolomeo, *Adv. Mater. Interfaces*, 2021, **8**, 2100149.
19 U. K. Panigrahi, P. K. Das, R. Biswal, V. Sathe, P. D. Babu, A. Mitra and P. Mallick, *J. Alloys Compd.*, 2020, **0925–8388**(20), 31413–155050.
20 P. Gupta, N. K. Pandey, K. Kumar and B. C. Yadav, *Sens. Actuators, A*, 2021, **319**, 112484.
21 S. K. Ranjit, S. A. Khalate and R. J. Deokate, *J. Alloys Compd.*, 2018, **734**, 89–111.
22 R. L. Wilson, C. Eugen Simion, A. Stanoiu, A. Taylor, S. Guldin, J. A. Covington, C. J. Carmaltand and C. S. Blackman, *ACS Sens.*, 2020, **5**, 1389–1397.
23 R. Sharma, A. D. Acharya, S. B. Shrivastava, M. Mishra Patidar, G. Mohan, T. Shripathi and V. Ganesan, *Optik*, 2016, **127**(11), 4661–4668.

24 S. Dewan, M. Tomar, R. P. Tandon and V. Gupta, *J. Appl. Phys.*, 2017, **121**, 215307.
25 S. Kumar, P. Vats, S. Gautam, V. P. Gupta, K. D. Verma, K. H. Chae, M. Hashim and H. K. Choi, *Mater. Res. Bull.*, 2014, **59**, 377–381.
26 M. Shakil, U. Inayat and M. Tanveer, *J. Environ. Sci. Technol.*, 2023, **20**, 2021–2036.
27 M. Taeño, D. Maestre and A. Cremades, *Nanophotonics*, 2021, **10**(7), 1785–1799.
28 V. Soundharrajan, B. Sambandam, J. Song, S. Kim, J. Jo, P. T. Duong, S. Kim and V. Mathew, *J. Energy Chem.*, 2018, **27**(1), 300–305.
29 G. Vijayaprasath, R. Murugan, T. Mahalingam and G. Ravi, *J. Mater. Sci.: Mater. Electron.*, 2015, **26**, 7205–7213.
30 Y. Liu, H. Liu, Z. Chen, N. Kadasala, C. Mao, Y. Wang, Y. Zhang, H. Liu, Y. Liu, J. Yang and Y. Yan, *J. Alloys Compd.*, 2014, **604**, 281–285.
31 X. Jiang, Z. Wang, D. Qi, F. Zhang, F. You and C. Yao, *Eur. J. Inorg. Chem.*, 2018, **39**, 4345–4348.
32 T. Shi, Z. Song, Y. Lv, D. Zhu, L. Miao, L. Gan and M. Liu, *Chin. Chem. Lett.*, 2024, 109559.
33 Y. Zhang, Z. Song, L. Miao, Y. Lv, L. Gan and M. Liu, *Angew. Chem., Int. Ed.*, 2024, **63**, e202316835.